Analyzing direct dark matter detection data with unrejected background events by the AMIDAS website

To cite this article: Chung-Lin Shan 2012 *J. Phys.: Conf. Ser.* **384** 012006

View the article online for updates and enhancements.

Analyzing direct dark matter detection data with unrejected background events by the AMIDAS website

Chung-Lin Shan

Institute of Physics, Academia Sinica
No. 128, Sec. 2, Academia Road, Nankang, Taipei 11529, Taiwan, R.O.C.

E-mail: `clshan@phys.sinica.edu.tw`

Abstract. In this talk I have presented the data analysis results of extracting properties of halo WIMPs: the mass and the (ratios between the) spin–independent and spin–dependent couplings/cross sections on nucleons by the `AMIDAS` website by taking into account possible *unrejected* background events in the analyzed data sets. Although *non–standard* astronomical setup has been used to generate *pseudodata* sets for our analyses, it has been found that, *without* prior information/assumption about the local density and velocity distribution of halo Dark Matter, these WIMP properties have been reconstructed with $\sim 2\%$ to $\lesssim 30\%$ deviations from the input values.

1. Introduction

In order to extract properties of halo WIMPs (Weakly Interacting Massive Particles) by using data from direct Dark Matter detection experiments as model–independently as possible, we have developed a series of data analysis method for reconstructing the one–dimensional WIMP velocity distribution [1] as well as determining the WIMP mass [2], the spin–independent (SI) WIMP coupling on nucleons [3] and the ratios between different WIMP couplings/cross sections [4]. Moreover, in collaboration with the DAMNED (DArk Matter Network Exclusion Diagram) Dark Matter online tool [5], part of the ILIAS Project [6], the "`AMIDAS`" (A Model–Independent Data Analysis System) website for online simulation/data analysis has also been established [7, 8, 9].

In this article, in order to demonstrate the usefulness and powerfulness as well as the model–independence of the `AMIDAS` package for direct Dark Matter detection experiments, I will analyze *blindly* some *pseudodata* sets generated theoretically for different detector materials and present the reconstructed WIMP properties. This means that I will simply upload these data sets onto the `AMIDAS` website and follow the instructions to reconstruct different WIMP properties *without* using any information about the input setup used for generating the analyzed pseudodata. For cases in which some information about WIMPs (e.g., the mass m_χ) and/or Galactic halo (e.g., the local Dark Matter density ρ_0) is required, I will naively use the commonly used/favorite values for the data analyses. Moreover, due to the time limit on preparing the presentation for the CYNGUS 2011 workshop, in Ref. [10] we considered only the case of *null* background events. In this article, we have taken into account a small fraction of possible *unrejected* background events in the analyzed data sets [11, 12, 13, 14].

Results

Reconstructed WIMP mass

m_χ (GeV/c^2)	$m_{\chi,\ \mathrm{combined}}$	$m_{\chi,\ 2}$	$m_{\chi,\ 1}$	$m_{\chi,\ -1}$	$m_{\chi,\ \sigma}$
$m_{\chi,\ \mathrm{rec}}$	103.51	61.498	38.38	-7.8539	40.127
$m_{\chi,\ \mathrm{lo}}$	71.387	10.177	-45.407	-94.28	-15.399
$m_{\chi,\ \mathrm{hi}}$	160.09	104.57	89.033	91.43	139.58

Results

Reconstructed WIMP mass

m_χ (GeV/c^2)	$m_{\chi,\ \mathrm{combined}}$	$m_{\chi,\ 2}$	$m_{\chi,\ 1}$	$m_{\chi,\ -1}$	$m_{\chi,\ \sigma}$
$m_{\chi,\ \mathrm{rec}}$	129.25	61.537	39.296	-6.712	40.032
$m_{\chi,\ \mathrm{lo}}$	83.137	8.9695	-47.646	-92.861	-15.494
$m_{\chi,\ \mathrm{hi}}$	215.32	109.35	86.2	91.42	144.8

Figure 1. The reconstructed WIMP mass m_χ by means of the method introduced in Ref. [2] with a target combination of ^{28}Si + ^{76}Ge nuclei. Two forms of the elastic nuclear form factor given in Eqs. (1) and (2) have been used in the left and right frames, respectively.

After that I show the blindly reconstructed properties of halo WIMPs in Sec. 2, in Sec. 3 I will reveal the input setup and the background spectrum used for generating the analyzed data and compare the reconstructed results to them. Finally, I conclude in Sec. 4.

2. Reconstructed WIMP properties

In this section, I present the reconstructed WIMP properties analyzed by the `AMIDAS` website. While in each uploaded file there are *exactly* 50 data sets, in each data set there are *on average* 50 recorded events (i.e., 50 measured recoil energies); the exact number of total events is Poisson distributed. For simplicity, the experimental minimal and maximal cut–off energies have been set as 0 and 100 keV for all data sets.

In order to check the effect of using a "wrong" elastic nuclear form factor, two forms have been considered for the SI WIMP–nucleus cross section in our analyses. One is the simple exponential form:

$$F_{\mathrm{ex}}^2(Q) = e^{-Q/Q_0} \, . \tag{1}$$

Here Q is the recoil energy transferred from the incident WIMP to the target nucleus, Q_0 is the nuclear coherence energy given by $Q_0 = 1.5/m_\mathrm{N} R_0^2$, where $R_0 = \left[0.3 + 0.91 \left(m_\mathrm{N}/\mathrm{GeV} \right)^{1/3} \right]$ fm is the radius of the nucleus and m_N is the mass of the target nucleus. Meanwhile, we used also a more realistic analytic form for the elastic nuclear form factor:

$$F_{\mathrm{SI}}^2(Q) = \left[\frac{3 j_1(q R_1)}{q R_1} \right]^2 e^{-(qs)^2} \, . \tag{2}$$

Here $j_1(x)$ is a spherical Bessel function, $q = \sqrt{2 m_\mathrm{N} Q}$ is the transferred 3-momentum, for the effective nuclear radius we use
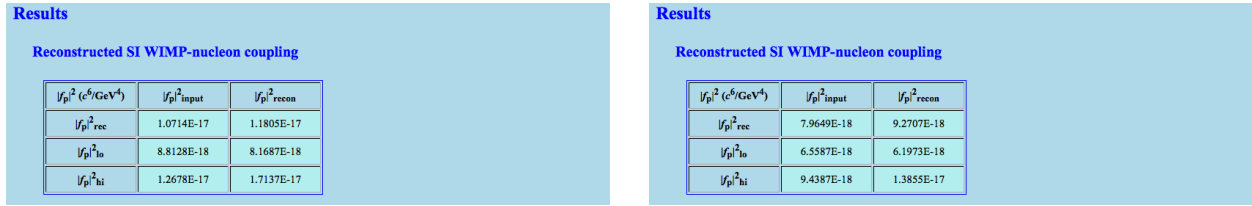
$$R_1 = \sqrt{R_A^2 - 5s^2} \tag{3}$$

with $R_A \simeq 1.2 \, A^{1/3}$ fm and a nuclear skin thickness $s \simeq 1$ fm. For the SD WIMP–nucleus cross section, we only used the "thin–shell" nuclear form factor:

$$F_{\mathrm{TS}}^2(Q) = \begin{cases} j_0^2(q R_1) \, , & \text{for } q R_1 \leq 2.55 \text{ or } q R_1 \geq 4.5 \, , \\ \text{const.} \simeq 0.047 \, , & \text{for } 2.55 \leq q R_1 \leq 4.5 \, . \end{cases} \tag{4}$$

2.1. WIMP mass m_χ

As one of the most important properties of halo WIMPs as well as the basic information for reconstructing other quantities in our model–independent analysis methods, I consider at first the determination of the WIMP mass m_χ by means of the method introduced in Ref. [2].

In Figs. 1 I show the reconstructed WIMP masses and the lower and upper bounds of their 1σ statistical uncertainties. The usual target combination of ^{28}Si + ^{76}Ge nuclei has been used

Results

Reconstructed SI WIMP-nucleon coupling

$\|f_{\mathrm{p}}\|^2$ (c^6/GeV^4)	$\|f_{\mathrm{p}}\|^2_{\mathrm{input}}$	$\|f_{\mathrm{p}}\|^2_{\mathrm{recon}}$
$\|f_{\mathrm{p}}\|^2_{\mathrm{rec}}$	1.0714E-17	1.1805E-17
$\|f_{\mathrm{p}}\|^2_{\mathrm{lo}}$	8.8128E-18	8.1687E-18
$\|f_{\mathrm{p}}\|^2_{\mathrm{hi}}$	1.2678E-17	1.7137E-17

Results

Reconstructed SI WIMP-nucleon coupling

$\|f_{\mathrm{p}}\|^2$ (c^6/GeV^4)	$\|f_{\mathrm{p}}\|^2_{\mathrm{input}}$	$\|f_{\mathrm{p}}\|^2_{\mathrm{recon}}$
$\|f_{\mathrm{p}}\|^2_{\mathrm{rec}}$	7.9649E-18	9.2707E-18
$\|f_{\mathrm{p}}\|^2_{\mathrm{lo}}$	6.5587E-18	6.1973E-18
$\|f_{\mathrm{p}}\|^2_{\mathrm{hi}}$	9.4387E-18	1.3855E-17

Figure 2. The reconstructed *squared* SI WIMP–nucleon coupling $|f_{\mathrm{p}}|^2$ by means of the method introduced in Ref. [3] with a ^{76}Ge target. The commonly used value of the local Dark Matter density $\rho_0 = 0.3$ GeV/cm^3 and a larger value of $\rho_0 = 0.4$ GeV/cm^3 as well as the elastic nuclear form factors given in Eqs. (1) and (2) have been used for estimating $|f_{\mathrm{p}}|^2$ in the left and right frames, respectively.

for this reconstruction, whereas two analytic forms of the elastic nuclear form factor given in Eqs. (1) and (2) have been used for determining m_χ in the left and right frames, respectively. While $m_{\chi,n}$ with $n = -1, 1, 2$ and $m_{\chi,\sigma}$ have been estimated by Eqs. (34) and (40) of Ref. [2], respectively, $m_{\chi,\mathrm{combined}}$ has been estimated by the χ^2–fitting defined in Eq. (51) of Ref. [2], which combines the estimators for $m_{\chi,n}$ and $m_{\chi,\sigma}$ with each other. The reconstructed WIMP mass $m_{\chi,\mathrm{combined}}$ as well as $m_{\chi,n}$ and $m_{\chi,\sigma}$ shown here have been corrected by the iterative Q_{max}–matching procedure described in Ref. [2].

It can be found here that, although all single estimators ($m_{\chi,n}$ with $n = -1, 1, 2$ and $m_{\chi,\sigma}$) give generally a (relatively lighter) WIMP mass of ~ 60 GeV or even lighter and a 1σ upper bound of ~ 140 GeV, the *mean* values of the combined (in principle, more reliable) results (second columns) of the reconstructed WIMP mass give $m_\chi \sim 115$ GeV with a *rough* 1σ upper (lower) bound of ~ 190 (80) GeV, or, equivalently,

$$m_\chi \simeq 115^{+75}_{-35} \text{ GeV} . \tag{5}$$

Moreover, the combined results with two different form factors show not only a large overlap between ~ 85 GeV and ~ 180 GeV, but also a good coincidence: comparing to the $\sim^{+75}_{-35}$ GeV 1σ statistical uncertainty and the $\sim^{+45}_{-30}$ GeV overlap, the difference between two median values is $\lesssim 30$ GeV! This indicates that, for the first approximation of giving/constraining the most plausible range of the WIMP mass with pretty few total events, the uncertainty on the nuclear form factor could be safely neglected.
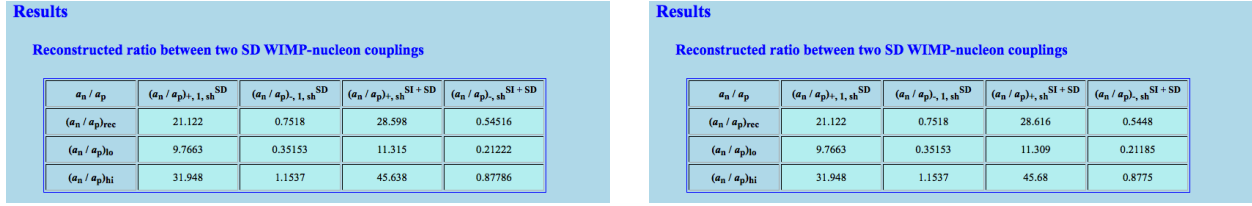
2.2. Spin–independent WIMP–nucleon coupling $|f_{\mathrm{p}}|^2$

Following the WIMP mass determination, I consider now the reconstruction of the SI WIMP coupling on nucleons $|f_{\mathrm{p}}|^2$ with a ^{76}Ge target [3] [1].

In Figs. 2 I show the reconstructed squared SI WIMP-nucleon couplings and the lower and upper bounds of their 1σ statistical uncertainties estimated by Eqs. (17) and (18) of Ref. [3] with an *assumed* (100 ± 10 GeV, labeled with the subscript "input") and the reconstructed (from Sec. 2.1, labeled with "recon") WIMP masses. The commonly used value of the local Dark Matter density $\rho_0 = 0.3$ GeV/cm^3 and a larger value of $\rho_0 = 0.4$ GeV/cm^3 [15, 16, 17] as well as the elastic nuclear form factors given in Eqs. (1) and (2) have been used for estimating $|f_{\mathrm{p}}|^2$ in the left and right frames, respectively.

Among these results, the *mean* value and the *overlap* of two most plausible results (estimated

---

[1] Remind that the theoretical prediction by most supersymmetric models that the SI scaler WIMP couplings on protons and on neutrons are (approximately) equal: $f_{\mathrm{p}} \simeq f_{\mathrm{n}}$ has been adopted in the `AMIDAS` package.

Results

Reconstructed ratio between two SD WIMP-nucleon couplings

a_n / a_p	$(a_n/a_p)_{+,1,\,\mathrm{sh}}^{\mathrm{SD}}$	$(a_n/a_p)_{-,1,\,\mathrm{sh}}^{\mathrm{SD}}$	$(a_n/a_p)_{+,\,\mathrm{sh}}^{\mathrm{SI+SD}}$	$(a_n/a_p)_{-,\,\mathrm{sh}}^{\mathrm{SI+SD}}$
$(a_n/a_p)_{\mathrm{rec}}$	21.122	0.7518	28.598	0.54516
$(a_n/a_p)_{\mathrm{lo}}$	9.7663	0.35153	11.315	0.21222
$(a_n/a_p)_{\mathrm{hi}}$	31.948	1.1537	45.638	0.87786

Results

Reconstructed ratio between two SD WIMP-nucleon couplings

a_n / a_p	$(a_n/a_p)_{+,1,\,\mathrm{sh}}^{\mathrm{SD}}$	$(a_n/a_p)_{-,1,\,\mathrm{sh}}^{\mathrm{SD}}$	$(a_n/a_p)_{+,\,\mathrm{sh}}^{\mathrm{SI+SD}}$	$(a_n/a_p)_{-,\,\mathrm{sh}}^{\mathrm{SI+SD}}$
$(a_n/a_p)_{\mathrm{rec}}$	21.122	0.7518	28.616	0.5448
$(a_n/a_p)_{\mathrm{lo}}$	9.7663	0.35153	11.309	0.21185
$(a_n/a_p)_{\mathrm{hi}}$	31.948	1.1537	45.68	0.8775

Figure 3. The reconstructed ratio between two SD WIMP–nucleon couplings, a_n/a_p, by means of two methods introduced in Ref. [4]. As usual, the elastic nuclear form factors given in Eqs. (1) and (2) have been used for determining a_n/a_p in the left and right frames, respectively.

with the reconstructed WIMP mass) give a *rough* 1σ range of

$$|f_p|^2 \simeq 1.05^{+0.33}_{-0.24} \times 10^{-17} \ \mathrm{GeV}^{-4} \,, \tag{6}$$

or, equivalently,

$$|f_p| \simeq 3.24^{+0.51}_{-0.37} \times 10^{-9} \ \mathrm{GeV}^{-2} \,. \tag{7}$$

Since the reconstructed WIMP mass given in Sec. 2.1 is $m_\chi \sim 115$ GeV, one can simply use the proton mass m_p to approximate the WIMP–proton reduced mass $m_{r,p}$ and give a reconstructed SI WIMP–nucleon cross section as [10]

$$\sigma^{\mathrm{SI}}_{\chi\mathrm{P}} = \left(\frac{4}{\pi}\right) m_{r,p}^2 |f_p|^2 \approx \left(\frac{4}{\pi}\right) m_p^2 |f_p|^2 \simeq 5.03^{+1.58}_{-1.15} \times 10^{-9} \ \mathrm{pb} \,. \tag{8}$$

2.3. Ratio of two spin–dependent WIMP–nucleon couplings a_n/a_p
In Figs. 3 I show the reconstructed a_n/a_p ratios and the lower and upper bounds of their 1σ statistical uncertainties estimated by Eqs. (2.7) and (2.12) of Ref. [4] with $n = 1$ as well as by Eqs. (3.16) and (3.20) of Ref. [4] at the shifted energy points [1, 4]. A combination of ^{19}F + ^{127}I targets has been used for the reconstruction of a_n/a_p under the assumption that the SD WIMP–nucleus interaction dominates over the SI one (labeled with the superscript "SD"), whereas a third target of ^{28}Si has been combined with ^{19}F and ^{127}I for the case of the general combination of both SI and SD WIMP interactions (labeled with the superscript "SI + SD").

It can be found that, firstly, the "+ (plus)" solutions of the a_n/a_p ratios given here are obviously too large to be the reasonable choice for a_n/a_p and the "− (minus)" solutions should be the correct ones[2]. Secondly, although the reconstructed results under the assumption of the SD dominant WIMP interaction (third columns) is in general *larger* than the (in principle more plausible) results obtained without such a prior assumption (last columns), one could still use the *mean* value and the *overlap* of these two results to give a *rough* 1σ range of

$$\frac{a_n}{a_p} \simeq 0.65^{+0.23}_{-0.30} \,. \tag{9}$$

2.4. Ratios of the SD and SI WIMP–nucleon couplings $\sigma^{\mathrm{SD}}_{\chi(\mathrm{p,n})}/\sigma^{\mathrm{SI}}_{\chi\mathrm{P}}$
In Figs. 4 I show the reconstructed $\sigma^{\mathrm{SD}}_{\chi(\mathrm{p,n})}/\sigma^{\mathrm{SI}}_{\chi\mathrm{P}}$ ratios and the lower and upper bounds of their 1σ statistical uncertainties estimated by Eqs. (3.9), (3.10) and (3.21) of Ref. [4] (with a_n/a_p estimated by Eq. (3.16) of Ref. [4]) as well as by Eqs. (3.25) and (3.29) of Ref. [4] at the shifted energy points. A combination of data sets of ^{19}F, ^{127}I and ^{28}Si targets (labeled with

[2] Remind that, as discussed in Ref. [4], the correct choice from the "+" and "−" solutions could be decided directly by the values of the group spins of protons and neutrons of the used target nuclei, $\langle S_{(\mathrm{p,n})} \rangle$.

Results

Reconstructed ratio between the SD and SI WIMP-proton cross sections

$\sigma_{\chi p}^{SD}/\sigma_{\chi p}^{SI}$	$(\sigma_{\chi p}^{SD}/\sigma_{\chi p}^{SI})_{+,\,sh}^{XYZ}$	$(\sigma_{\chi p}^{SD}/\sigma_{\chi p}^{SI})_{-,\,sh}^{XYZ}$	$(\sigma_{\chi p}^{SD}/\sigma_{\chi p}^{SI})_{sh}^{XY}$
$(\sigma_{\chi p}^{SD}/\sigma_{\chi p}^{SI})_{rec}$	16573	818120	963240
$(\sigma_{\chi p}^{SD}/\sigma_{\chi p}^{SI})_{lo}$	-2740	557440	623450
$(\sigma_{\chi p}^{SD}/\sigma_{\chi p}^{SI})_{hi}$	36176	1104800	1290000

Reconstructed ratio between the SD and SI WIMP-neutron cross sections

$\sigma_{\chi n}^{SD}/\sigma_{\chi p}^{SI}$	$(\sigma_{\chi n}^{SD}/\sigma_{\chi p}^{SI})_{+,\,sh}^{XYZ}$	$(\sigma_{\chi n}^{SD}/\sigma_{\chi p}^{SI})_{-,\,sh}^{XYZ}$	$(\sigma_{\chi n}^{SD}/\sigma_{\chi p}^{SI})_{sh}^{XY}$
$(\sigma_{\chi n}^{SD}/\sigma_{\chi p}^{SI})_{rec}$	13619000	241030	387610
$(\sigma_{\chi n}^{SD}/\sigma_{\chi p}^{SI})_{lo}$	9274200	-45707	210250
$(\sigma_{\chi n}^{SD}/\sigma_{\chi p}^{SI})_{hi}$	18393000	551530	565850

Results

Reconstructed ratio between the SD and SI WIMP-proton cross sections

$\sigma_{\chi p}^{SD}/\sigma_{\chi p}^{SI}$	$(\sigma_{\chi p}^{SD}/\sigma_{\chi p}^{SI})_{+,\,sh}^{XYZ}$	$(\sigma_{\chi p}^{SD}/\sigma_{\chi p}^{SI})_{-,\,sh}^{XYZ}$	$(\sigma_{\chi p}^{SD}/\sigma_{\chi p}^{SI})_{sh}^{XY}$
$(\sigma_{\chi p}^{SD}/\sigma_{\chi p}^{SI})_{rec}$	16585	819680	968370
$(\sigma_{\chi p}^{SD}/\sigma_{\chi p}^{SI})_{lo}$	-2736.9	558420	626960
$(\sigma_{\chi p}^{SD}/\sigma_{\chi p}^{SI})_{hi}$	36213	1107100	1297100

Reconstructed ratio between the SD and SI WIMP-neutron cross sections

$\sigma_{\chi n}^{SD}/\sigma_{\chi p}^{SI}$	$(\sigma_{\chi n}^{SD}/\sigma_{\chi p}^{SI})_{+,\,sh}^{XYZ}$	$(\sigma_{\chi n}^{SD}/\sigma_{\chi p}^{SI})_{-,\,sh}^{XYZ}$	$(\sigma_{\chi n}^{SD}/\sigma_{\chi p}^{SI})_{sh}^{XY}$
$(\sigma_{\chi n}^{SD}/\sigma_{\chi p}^{SI})_{rec}$	13645000	241240	389540
$(\sigma_{\chi n}^{SD}/\sigma_{\chi p}^{SI})_{lo}$	9290500	-46018	211340
$(\sigma_{\chi n}^{SD}/\sigma_{\chi p}^{SI})_{hi}$	18431000	552080	568600

Figure 4. The reconstructed ratios between the SD and SI WIMP–nucleon couplings, $\sigma_{\chi(p,n)}^{SD}/\sigma_{\chi P}^{SI}$, by means of two methods introduced in Ref. [4]. As usual, the elastic nuclear form factors given in Eqs. (1) and (2) have been used for determining $\sigma_{\chi(p,n)}^{SD}/\sigma_{\chi P}^{SI}$ in the left and right frames, respectively.

the superscript "XYZ") and that of data sets of ^{23}Na or ^{131}Xe with the (common) one of ^{76}Ge (labeled with the superscript "XY") have been used and the *mean* value and the *overlap* of these two results give a *rough* 1σ range of

$$\frac{\sigma_{\chi P}^{SD}}{\sigma_{\chi P}^{SI}} \simeq 8.94^{+2.13}_{-2.67} \times 10^5\,, \qquad\qquad \frac{\sigma_{\chi n}^{SD}}{\sigma_{\chi P}^{SI}} \simeq 3.16^{+2.36}_{-1.05} \times 10^5\,. \qquad (10)$$

Then, firstly, from these results one can further obtain that [10][3]

$$\left|\frac{a_n}{a_p}\right| \simeq 0.59^{+0.23}_{-0.13}\,. \qquad (11)$$

Secondly, combining the results in Eq. (10) with $\sigma_{\chi P}^{SI}$ given in Eq. (8), one can obtain that [10]

$$\sigma_{\chi P}^{SD} \simeq 4.50^{+1.77}_{-1.69} \times 10^{-3}\ \text{pb}\,, \qquad\qquad \sigma_{\chi n}^{SD} \simeq 1.59^{+1.08}_{-0.64} \times 10^{-3}\ \text{pb}\,. \qquad (12)$$

These results give in turn that [10]

$$|a_p| = 0.112^{+0.022}_{-0.021}\,, \qquad\qquad |a_n| = 0.067^{+0.023}_{-0.013}\,. \qquad (13)$$

On the other hand, one can also use the reconstructed a_n/a_p ratio given in Eq. (9) and *one* of the two results given in Eq. (12) to obtain that [10]

$$\sigma_{\chi P}^{SD} \simeq 3.76^{+3.69}_{-3.81} \times 10^{-3}\ \text{pb}\,, \qquad\qquad \sigma_{\chi n}^{SD} \simeq 1.90^{+1.54}_{-1.89} \times 10^{-3}\ \text{pb}\,. \qquad (14)$$

These results can also give that

$$|a_p| \simeq 0.103^{+0.050}_{-0.052}\,, \qquad\qquad |a_n| \simeq 0.073^{+0.030}_{-0.036}\,. \qquad (15)$$

It can be found that, not surprisingly, the statistical uncertainties on the reconstructed $\sigma_{\chi(p,n)}^{SD}$ given in Eq. (14) are ~ 2 or 3 times larger than those given in Eq. (12): Since $\sigma_{\chi(p,n)}^{SD}/\sigma_{\chi P}^{SI}$

---

[3] Remind that the results given in the second and third columns of the tables in Figs. 4 are reconstructed with the a_n/a_p ratio given in the last columns of the tables in Figs. 3.

reconstructed with the F + I + Si combination involve already the reconstructed a_n/a_p ratio given in Eq. (9), the uncertainties on $\sigma^{SD}_{\chi(p,n)}$ given in Eq. (14) are thus *overestimated*. Secondly, the reconstructed a_n/a_p ratio given in Eqs. (9) and (11) and the reconstructed $\sigma^{SD}_{\chi(p,n)}$ given in Eqs. (12) and (14) seem to match to each other pretty well.

The analyses given here show that, firstly, once one can estimate the SI WIMP–nucleon coupling/cross section, $|f_p|$ or $\sigma^{SI}_{\chi p}$, and (one of) the ratios between the SD and SI WIMP–nucleon cross sections, and/or the ratio between two SD WIMP–nucleon couplings, the other couplings/cross sections could in principle be estimated. Secondly, the WIMP couplings/cross sections estimated in different way would be self–cross–checks to each other and the (in)compatibility between the reconstructed results would also help us to check the usefulness of the analyzed data sets offered from different experiments with different detector materials [14].

3. Input setup for generating pseudodata

In Table 1 I give finally the input setup for generating the pseudodata sets used in the analyses demonstrated in the previous section. For comparison, the reconstructed results shown in the previous section are also summarized here.

For generating WIMP signals, we used the commonly used form for the nuclear form factor given in Eq. (2) with another often used analytic form for R_1:

$$R_1 = \sqrt{R_A^2 + \left(\tfrac{7}{3}\right)\pi^2 r_0^2 - 5s^2} \qquad (16)$$

with $R_A \simeq (1.23\, A^{1/3} - 0.6)$ fm, $r_0 \simeq 0.52$ fm, $s \simeq 0.9$ fm. Moreover, the shifted Maxwellian velocity distribution:

$$f_{1,\mathrm{sh}}(v) = \frac{1}{\sqrt{\pi}}\left(\frac{v}{v_e v_0}\right)\left[e^{-(v-v_e)^2/v_0^2} - e^{-(v+v_e)^2/v_0^2}\right] \qquad (17)$$

with the Sun's Galactic orbital velocity $v_0 = 230$ km/s has been used; v_e is the *time–dependent* Earth's velocity in the Galactic frame:

$$v_e(t) = v_0 \left[1.05 + 0.07\cos\left(\frac{2\pi(t - t_p)}{1\ \mathrm{yr}}\right)\right], \qquad (18)$$

where the date on which the Earth's velocity relative to the WIMP halo is maximal has been set as $t_p = 140$ d. In addition, different from our setup used in Ref. [10], the experimental running date has been set as $t_{\mathrm{expt}} = 100$ d and thus $v_e(t_{\mathrm{expt}}) = 254$ km/s, much larger than the usually used values: 200 km/s $\leq v_e \leq$ 240 km/s. Although these values for the astronomical setup are *non–standard*, we would like to stress that, as shown in the previous section and Table I, such a non–standard halo (model) would not affect the reconstructed results, since for using the AMIDAS package and website to analyze (real) data sets, one needs only the form factors for SI and/or SD WIMP–nucleaus cross sections, prior knowledge/assumptions about the WIMP velocity distribution $f_1(v)$ and local density ρ_0 (except the estimation of the SI WIMP–nucleon coupling $|f_p|^2$) are *not required*.

On the other hand, for generating background events, the target–dependent exponential form for the residue background spectrum introduced in Ref. [11]:

$$\left(\frac{dR}{dQ}\right)_{\mathrm{bg,ex}} = \exp\left(-\frac{Q/\mathrm{keV}}{A^{0.6}}\right) \qquad (19)$$

| Property	Reconstructed value	Input/Estimated value	Remarks
m_χ	115^{+75}_{-35} GeV	130 GeV	
$\sigma^{\rm SI}_{\chi \rm P}$	$5.03^{+1.58}_{-1.15} \times 10^{-9}$ pb	4×10^{-9} pb	$f_{\rm n} = f_{\rm p}$
$|f_{\rm p}|^2$	$1.05^{+0.33}_{-0.24} \times 10^{-17}$ GeV^{-4}	9.305×10^{-18} GeV^{-4}	†
$|f_{\rm p}|$	$3.24^{+0.51}_{-0.37} \times 10^{-9}$ GeV^{-2}	3.050×10^{-9} GeV^{-2}	†
$a_{\rm p}$ $a_{\rm n}$	$0.112^{+0.022}_{-0.021}$ $0.067^{+0.023}_{-0.013}$	0.1 0.07	
$a_{\rm n}/a_{\rm p}$	$0.65^{+0.23}_{-0.30}, 0.59^{+0.23}_{-0.13}$	0.7	
$\sigma^{\rm SD}_{\chi \rm P}$ $\sigma^{\rm SD}_{\chi \rm n}$	$4.50^{+1.77}_{-1.69} \times 10^{-3}$ pb $1.59^{+1.08}_{-0.64} \times 10^{-3}$ pb	3.51×10^{-3} pb 1.72×10^{-3} pb	† †
$\sigma^{\rm SD}_{\chi \rm P}/\sigma^{\rm SI}_{\chi \rm P}$ $\sigma^{\rm SD}_{\chi \rm n}/\sigma^{\rm SI}_{\chi \rm P}$	$8.94^{+2.13}_{-2.67} \times 10^5$ $3.16^{+2.36}_{-1.05} \times 10^5$	8.77×10^5 4.30×10^5	† †
$F^2_{\rm SI}(Q)$ $F^2_{\rm SD}(Q)$		$F^2_{\rm SI}(Q)$ in Eq. (2) $F^2_{\rm TS}(Q)$ in Eq. (4)	‡
ρ_0		0.4 GeV/cm^3	
$t_{\rm p}$ $t_{\rm expt}$		140 d 100 d	‡
v_0 $v_{\rm max}$ $v_{\rm e}(t_{\rm expt})$		230 km/s 600 km/s 253.9 km/s	‡
$r_{\rm bg}$		0.12	‡

Table 1. The input setup for generating the pseudodata sets used in the analyses demonstrated in this article. The theoretically estimated values and the reconstructed results are also given. †: estimated for 130 GeV m_χ; ‡: different from Ref. [10].

has been used. Here A is the atomic mass number of the target nucleus; the power index of A, 0.6, is an empirical constant, which has been chosen so that the exponential background spectrum is somehow similar to, but still different from the expected recoil spectrum of the target nuclei (see Figs. 5)[4]. Meanwhile, considering possible radioactivity with a characteristic energy, we combined the exponential background spectrum in Eq. (19) with a Gaussian excess:

$$\left(\frac{dR}{dQ}\right)_{\rm bg, Gau} = \frac{r_{\rm Gau}}{\sqrt{2\pi}\,(\sigma_{Q,\rm bg}/{\rm keV})} \exp\left[-\frac{(Q - Q_{\rm bg,peak})^2}{2\sigma^2_{Q,\rm bg}}\right], \tag{20}$$

[4] Note that, among different possible choices the atomic mass number A has been chosen as the simplest, unique characteristic parameter in the general analytic form (19) for defining the residue background spectrum for *different* target nuclei. However, it does *not* mean that the (superposition of the real) background spectra would depend simply/primarily on A or on the mass of the target nucleus, $m_{\rm N}$.
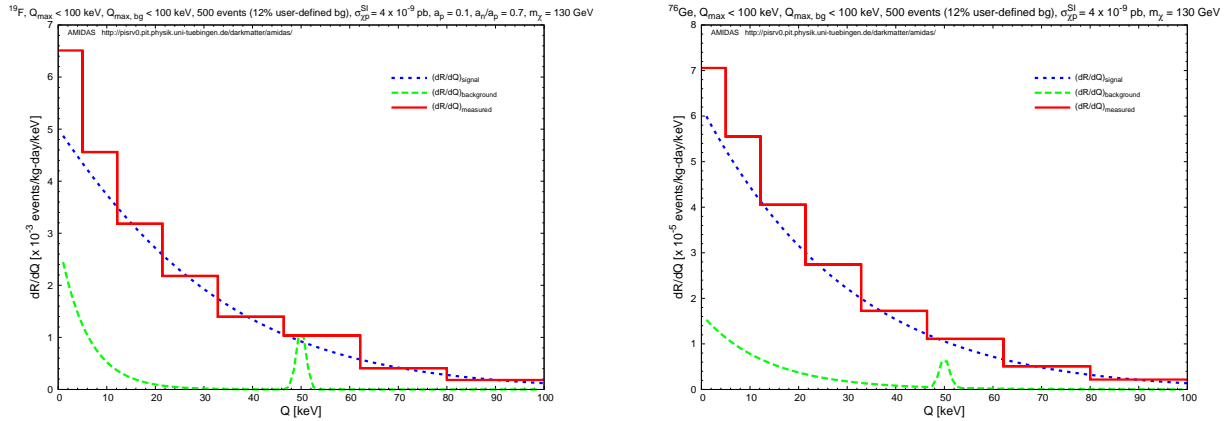
Figure 5. Measured energy spectra (solid red histograms) for a ^{19}F (left) and a ^{76}Ge (right) targets. The dotted blue curves are the elastic WIMP–nucleus scattering spectra, whereas the dashed green curves are the exponential background spectra combined with the Gaussian excesses ($r_{\rm Gau} = 1$, $Q_{\rm bg,peak} = 50$ keV and $\sigma_{Q,\rm bg} = 1$ keV) and normalized to fit to the chosen background ratio $r_{\rm bg} = 12\%$. See the text for further details.

where $Q_{\rm bg,peak}$ and $\sigma_{Q,\rm bg}$ are the characteristic energy and energy dispersion of this background excess, respectively; $r_{\rm Gau}$ is the ratio of this Gaussian excess to the exponential spectrum.

In Figs. 5 I show the measured energy spectra (solid red histograms) for a ^{19}F (left) and a ^{76}Ge (right) targets. The dotted blue curves are the elastic WIMP–nucleus scattering spectra, whereas the dashed green curves are the exponential background spectra given in Eq. (19) combined with the Gaussian excesses given in Eq. (20) ($r_{\rm Gau} = 1$, $Q_{\rm bg,peak} = 50$ keV and $\sigma_{Q,\rm bg} = 1$ keV for both targets), which have been normalized so that the ratios of the areas under the background spectra to those under the (dotted blue) WIMP scattering spectra are equal to the background–signal ratio ($r_{\rm bg} = 12\%$) in the whole data sets. The experimental threshold energies have been assumed to be negligible and the maximal cut–off energies are set as 100 keV. 500 total events on average in one experiment have been simulated.

It can be seen here that[5], firstly, due to the contribution of the unrejected background events in low energy ranges ($Q \lesssim 20$ keV for ^{19}F and $Q \lesssim 40$ keV for ^{76}Ge), the counting rates at the first energy bins (one of the two important quantities required in our model–independent data analyses) have been (strongly) overestimated. Secondly, the Gaussian background excesses around $Q = 50$ keV cause clearly overestimates of the event rates, which would not only contribute (significantly) to the estimates of $I_n = \sum_{\rm all\ events} Q_i^{(n-1)/2}/F^2(Q_i)$ [1], but also cause a larger statistical fluctuation [2].

Nevertheless, our results obtained by analyzing pseudodata sets of $\mathcal{O}(50)$ total events showed that, firstly, the WIMP mass given in Eq. (5) can match the input value very well: the deviations between the input and the reconstructed values with different assumed nuclear form factors are $\lesssim 20\%$ ($\lesssim 30$ GeV). As discussed earlier, this indicates that, for the first approximation of giving/constraining the most plausible range of the WIMP mass with pretty few total events, the uncertainty on the nuclear form factor could be safely neglected.

Secondly, all WIMP–nucleon couplings/cross sections as well as the ratios between them have also been reconstructed with $\sim 2\%$ to $\lesssim 30\%$ deviations from the input/theoretically estimated values. Although the SI WIMP coupling $|f_{\rm p}|$ estimated with the larger (input) local Dark Matter density (right frame of Figs. 2) could be underestimated [3], one can at least give an upper bound

---

[5] More detailed illustrations and discussions about the effects of residue background events on the measured energy spectrum can be found in Refs. [11, 14].

on $|f_{\rm p}|$. Moreover, by combining different methods for estimating different (ratios between the) WIMP couplings/cross sections, one could in principle observe/confirm the (in)compatibility between these results and probably correct the reconstructed values.

4. Summary

In this article I demonstrated the data analysis results of extracted WIMP properties by using theoretically generated pseudodata for different target nuclei, taking into account some unrejected background events mixed in the analyzed data sets. As an extension as well as the complementarity of our earlier theoretical works, I combined reconstructed results of the (ratios between different) WIMP couplings/cross sections on nucleons to estimate each *individual* coupling/cross section. Hopefully, the `AMIDAS` package and website as well as this demonstration can help our experimental colleagues to analyze their *real* direct detection data in the near future and to determine (at least rough ranges of) properties of halo Dark Matter particles.

References

[1] Drees M and Shan C-L 2007 Reconstructing the velocity distribution of WIMPs from direct dark matter detection data *J. Cosmol. Astropart. Phys.* JCAP06(2007)011 (*Preprint* astro-ph/0703651)
[2] Drees M and Shan C-L 2008 Model–independent determination of the WIMP mass from direct dark matter detection data *J. Cosmol. Astropart. Phys.* JCAP06(2008)012 (*Preprint* 0803.4477)
[3] Shan C-L 2011 Estimating the spin–independent WIMP–nucleon coupling from direct dark matter detection data (*Preprint* 1103.0481)
[4] Shan C-L 2011 Determining ratios of WIMP–nucleon cross sections from direct dark matter detection data *J. Cosmol. Astropart. Phys.* JCAP07(2011)005 (*Preprint* 1103.0482)
[5] http://pisrv0.pit.physik.uni-tuebingen.de/darkmatter/index1.html
[6] http://www-ilias.cea.fr/
[7] http://pisrv0.pit.physik.uni-tuebingen.de/darkmatter/amidas/
[8] Shan C-L 2010 The `AMIDAS` website: an online tool for direct dark matter detection experiments *AIP Conf. Proc.* **1200** 1031 (*Preprint* 0909.1459)
[9] Shan C-L 2009 Uploading user–defined functions onto the `AMIDAS` website (*Preprint* 0910.1971)
[10] Shan C-L 2011 Analyzing direct dark matter detection data on the `AMIDAS` website (*Preprint* 1109.0125)
[11] Chou Y-T and Shan C-L 2010 Effects of residue background events in direct dark matter detection experiments on the determination of the WIMP mass *J. Cosmol. Astropart. Phys.* JCAP08(2010)014 (*Preprint* 1003.5277)
[12] Shan C-L 2010 Effects of residue background events in direct dark matter detection experiments on the reconstruction of the velocity distribution function of halo WIMPs *J. Cosmol. Astropart. Phys.* JCAP06(2010)029 (*Preprint* 1003.5283)
[13] Shan C-L 2011 Effects of residue background events in direct dark matter detection experiments on the estimation of the spin–independent WIMP–nucleon coupling (*Preprint* 1103.4049)
[14] Shan C-L 2011 Effects of residue background events in direct dark matter detection experiments on the determinations of ratios of WIMP–nucleon cross sections (*Preprint* 1104.5305)
[15] Catena R and Ullio P 2010 A novel determination of the local dark matter density *J. Cosmol. Astropart. Phys.* JCAP08(2010)004 (*Preprint* 0907.0018)
[16] Salucci P, Nesti F, Gentile G and Martins C F 2010 The dark matter density at the sun's location *Astron. Astrophys.* **523** A83 (*Preprint* 1003.3101)
[17] Pato M, Agertz O, Bertone G, Moore B and Teyssier R 2010 Systematic uncertainties in the determination of the local dark matter density *Phys. Rev.* D **82** 023531 (*Preprint* 1006.1322)